16th World Conference on Earthquake Engineering, 16WCEE 2017
Santiago Chile, January 9th to 13th 2017
Paper N° 4310 (Abstract ID)
Registration Code: S-R1462611862

EXPERIMENTAL AND NUMERICAL ASSESSMENT OF THE BEHAVIOUR OF RuCFST MEMBERS UNDER MONOTONIC AND CYCLIC BENDING

Y. Jiang[(1)], A. Silva[(2)], J. M. Castro[(3)], R. Monteiro[(4)] and N. Silvestre[(5)]

[(1)] *PhD Candidate, Istituto Universitario di Studi Superiori di Pavia, Italy, yadong.jiang@umeschool.it*
Researcher, Faculty of Engineering, University of Porto, Portugal, yadong.jiang@fe.up.pt
[(2)] *Researcher, Faculty of Engineering, University of Porto, Portugal, ajms@fe.up.pt*
[(3)] *Assistant Professor, Faculty of Engineering, University of Porto, Portugal, miguel.castro@fe.up.pt*
[(4)] *Assistant Professor, Istituto Universitario di Studi Superiori di Pavia, Italy, ricardo.monteiro@iusspavia.it*
[(5)] *Associate Professor, Technical University of Lisbon, Portugal, nsilvestre@tecnico.ulisboa.pt*

Abstract

The main objective of the research presented in this paper is to investigate the structural behaviour of Concrete Filled Steel Tube (CFST) columns made with Rubberized Concrete (RuC), and to identify behavioural differences between this type of composite members and typical CFST members made with standard concrete (StdC), namely in terms of the influence of the rubber aggregate replacement ratio on member strength, ductility, and energy dissipation capacity. The paper describes the preparation and development of an experimental campaign (Silva *et al* [1]), which involves the testing of 36 specimens of different cross-section types. The definition of the test campaign considered a number of parameters, namely cross-section slenderness, aggregate replacement ratio, axial load level and lateral loading type. A special device was developed as part of an innovative testing setup, aimed at reducing both the cost and preparation time of the specimens. The specimens were tested under both monotonic and cyclic lateral loading conditions and considering different levels of normalized axial load. This paper also describes the comparison of the test results with codified design provisions, namely with Eurocode 4 [2]. Additionally, an advanced numerical model for CFST columns is proposed using the finite element software ABAQUS [3], aimed at the accurate modelling of CFST behaviour in monotonic and cyclic bending, simple or combined with compression. A concrete damage plasticity model was adopted to represent the concrete damage under cyclic loading. A procedure was developed to take into account the steel tube's initial imperfection in the numerical analysis, and no significant sway of CFST behaviour in bending. The validity of the developed finite element model was examined by comparing the experimental results of the 36 CFST columns with the numerical results. It was found that, for both monotonic and cyclic lateral loading, not only the numerical test results show a good correlation, but also the local buckling of the steel tube is accurately captured by the model. Conservative prediction was found when compared the design capacity with Eurocode 4 [2] for both circular and square/rectangular CFST. An over-strength phenomenon was also indicated by the test results of circular CFST under monotonic bending.

Keywords: CFST; Experimental; Rubberized Concrete; Numerical Modelling

1. Introduction

In recent years, the use of concrete filled steel tubes (CFSTs) has increased in many modern structures. One of the key benefits of CFSTs is the confinement effect of the concrete provided by the steel tube. Unlike typical reinforced concrete members, CSFT members can make full use of the concrete material as it is entirely encased by steel tube. The steel tube can not only assist in the axial bearing capacity of the member, but also provide confinement to the concrete core. This leads to lighter and more cost efficient solutions than reinforced concrete. Moreover, the trial-axial compression stress state of the CFST core can prevent the brittle behaviour of the material. From a structural point of view, the concrete core has the ability to delay local buckling of the steel tube increasing therefore the ductility of the member.

The main objectives of this research are to 1) perform the experimental study to validate the flexural behaviour of CFST columns under both monotonic and cyclic loading; 2) study the applicability of combining rubberized concrete with steel tube; 3) develop and calibrate an reliable numerical model to reproduce the CFST column's bending behaviour; and 4) review the Eurocode 4 [2] design procedure based on the test results.

2. Preparation of the Test Campaign

The main parameters to be studied in the experimental campaign are: 1) cross-section shape, 2) cross-section slenderness, 3) rubberized concrete, 4) axial load. All the remaining parameters are kept constant. By combining the 4 aforementioned parameters, in total, 36 CFST columns are adopted to be test in the lab, as shown in Table 1.

Table 1 – Specimen list

No.	Steel tube	D [mm]		t [mm]	D/t	%RuC	Axial Load P/P0	Lateral Load Type
1 - 4	C219×3	219.1		3	73.0	15%	0% 15%	Monotonic Cyclic
5 - 16	C219×5	219.1		5	43.8	0 % 5% 15%		
No.	Steel tube	B [mm]		t [mm]	D/t [mm]	%RuC	Axial Load P/P0	Lateral Load Type
17 - 20	S180×3	180		3	60.0	15%	0% 15%	Monotonic Cyclic
21 - 32	S200×10	200		10	20.0	0 % 5% 15%		
No.	Steel tube	B [mm]	H [mm]	t [mm]	D/t [mm]	%RuC	Axial Load P/P0	Lateral Load Type
33 - 36	R250×150×12	250	150	12	20.8	15%	0% 15%	Monotonic Cyclic

2.1 Selection of the steel tube size

The experimental test campaign aims to investigate three types of steel tube sections, circular section, rectangular section and square section. For circular and rectangular sections, both ductile and non-ductile behaviour are desired to be achieved in the experiment. A cross-section slenderness ratio limitation from Eurocode 8 [4] has been taken into consideration, as shown in Table 2. In total, 5 different tube section sizes are adopted in this test, as shown in Table 3.

Table 2 – Relationship between behaviour factor and limits of wall slenderness from Eurocode 8 [4]

Ductility Class of Structure	DCM		DCH
Reference value of behaviour factor (q)	$q \leq 1.5$ - 2	1.5 - 2 < q < 4	$q > 4$
Filled Rectangular Section h/t limits:	52ε	38ε	24ε

Filled Circular Section *d/t* limits:	$90\varepsilon^2$	$85\varepsilon^2$	$80\varepsilon^2$

Where

$\varepsilon = \sqrt{f_y / 235}$

d/t and *h/t* are the ratio between the maximum external dimension and the wall thickness.

2.2 Steel properties

All steel tubes used in the test campaign are cold-formed. To evaluate the material mechanical properties, and considering that each tube of the same steel section type comes from the same lot, tensile testing of three steel coupons taken from a set of specimens was performed. Table 3 provides a comparison between the average steel mechanical properties, in terms of steel yield strength, f_y, and ultimate strength, f_u.

Table 3 – Average steel properties of the tubes

Steel tube section	C219×3	C219×5	S180×3	S200×10	R250×150×12
f_y [MPa]	308	393	325	490	575
f_u [MPa]	373	485	404	524	590

2.3 Concrete properties

Two kinds of rubberized concrete (RuC5% and RuC15%) and one standard concrete (StdC) were considered in the study. For rubberized concrete, two levels of aggregate replacement ratio (β), 5% and 15%, were used in the test campaign, by substituting only the largest range of aggregate size, 4/10 G_C85/20, with a percentage of the total amount of normal aggregate used in a given mixture. The mixing ratios for each concrete type are summarized in Table 4. Additionally, the table shows the average cube strength, obtained from the testing of three concrete cubes per mixture, corresponding to the three concrete types used in the test campaign. The tested concrete cubes were taken during steel tube pouring process and tested at 28 days of age.

Table 4 – Concrete properties

	Water [l/m^3]	Cement [kg/m^3]	0/4 GF85 [kg/m^3]	4/10 GC85/20 [kg/m^3]	Rubber [kg/m^3]	f_c [MPa]
StdC	216	420	551	1072	-	53
RuC5%	216	420	551	1019	54	39
RuC15%	227	420	542	896	158	20

2.4 Test setup

In the test, all the specimens are desired to have a fully restrained base with one vertical constant force and one horizontal displacement applied at the top. Fig. 2 shows the test setup and the two load actuators. A special steel box was designed to reduce the test costs and speed up the test process, as shown in Fig. 1. A 50mm thick steel box with an internal size of 750×750 mm is weld to a 60mm thick steel base plate. Five stiffeners are welded on each side of the box in order to stiffen the connection between the wall plates and the base plate. The core part of the box has custom-made high strength steel bolts and nuts. Each steel bolt is 100 mm long with an additional Ø 110 mm hexagon cap on the top to increase the contact area between the bolt and the specimen. 4 Ø 110 mm steel nuts with a thickness of 70 mm are welded to the steel wall, to connect with the bolts. Upon preparation of the specimen, one should position the specimen in the centre of the steel box, and unscrew the bolts until the bolt caps have a full contact with the specimen. One main drawback of the box is that, due to the layout of the bolts, only rectangular and square specimens can be installed and laterally restrained. Therefore, for circular steel tubes,

additional steel plates are welded at the bottom part of the tube in order to allow a similar connection to the box constraint mechanism, as shown in Fig. 3.

The specimens were tested under constant axial load and monotonic or cyclic increasing lateral displacement. Due to the characteristics of the test setup, the specimen test length was approximately 1.35m. The axial load N_0 was applied on some of the specimens and maintained constant throughout the test by a 750kN maximum capacity actuator. The lateral loading was based on the SAC cyclic loading protocol [5], in which six cycles are imposed for specimen drift ratios $\theta = 0.375\%$, $\theta = 0.50\%$ and $\theta = 0.75\%$, four cycles at $\theta = 1\%$, and two cycles for the remaining levels of θ with 1% increment. Due to the stroke limit of the actuator, displacement levels were limited to a maximum of ±150mm for pure bending and ±70mm for test combined with axial load. The rotation of the specimen's base section was measured to account for the rigid body rotation at evaluation of the effective top lateral displacement. Testing was conducted either up to specimen failure or until the actuator range limits were reached. It should be noted that, the position of vertical actuator was fixed and pointed to the centre of the base section during the test, thus there was no P-Δ effects in the test.

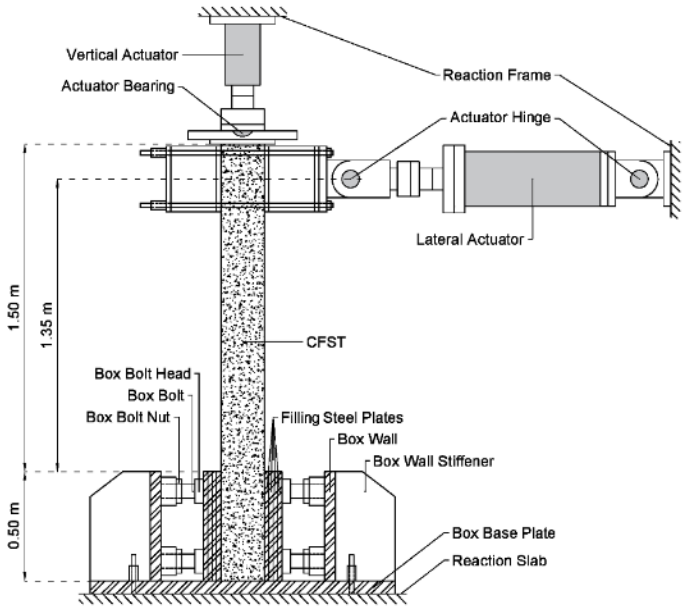

Fig. 2 – Test setup

Fig. 1 – Designed steel box

Fig. 3 – Circular CFST detail

3. Test results

3.1 Local buckling and failure mode

In all the specimens tested under monotonic lateral loading, combined or not with a constant axial load, a typical local plastic mode consisting of outward buckling was observed. As far as the cyclic lateral loading tests are concerned, all specimens without axial loading exhibited a failure mode characterized by fracture of the steel section after very significant local buckling of the tube wall, with a clear influence on the global behaviour of the specimen. Fig. 4 and Fig. 5 show the yield mechanism and failure mode for monotonic and cyclic lateral loading, respectively.

(a) (b)

Fig. 4 – Local buckling of the circular(a)/rectangular(b) CFST in a monotonic test

(a) (b)

Fig. 5 – Fracture of the circular(a)/rectangular(b) CFST during a cyclic test

3.2 Influence of loading type

Fig. 6 and Fig. 7 show the plots of lateral force vs drift ratio, in which two CFSTs with the same configuration were tested under monotonic and cyclic load, respectively. In general, all members under monotonic bending exhibited a very ductile behaviour, even after the occurrence of local buckling. No strength degradation was found for almost all specimens combined with or without axial load. Differently from the monotonic bending behaviour, strength degradation was observed for CFSTs under cyclic loading, and thus, the bending capacity is lower than one obtained from the corresponding monotonic test. Significant pinching effects were visible in cyclic tests, which were more pronounced for the cross-section with higher slenderness. It can also be found that, compared to the circular CFST, the rectangular members appeared to have an earlier strength degradation and a larger strength degradation gradient.

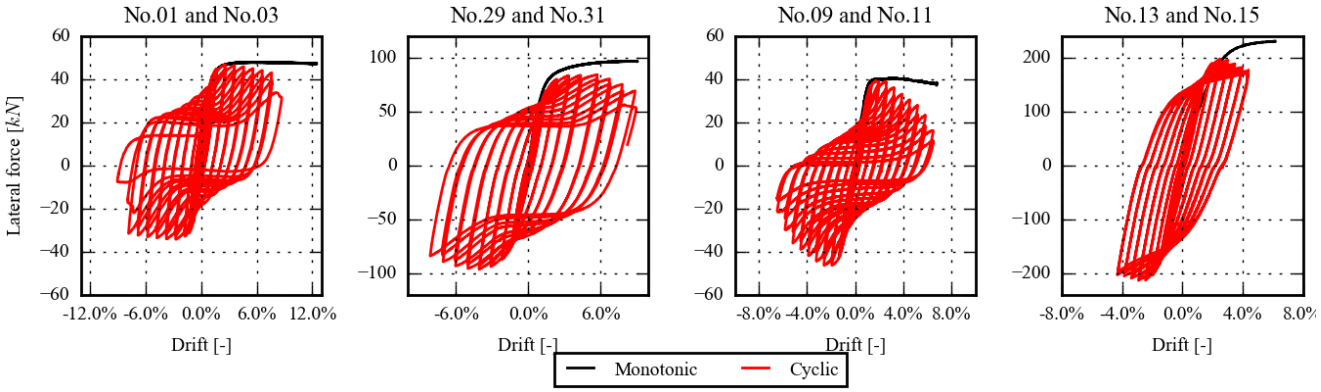

Fig. 6 – Test results of circular specimens No.01, No.03, No.29 and No.31

Fig. 7 – Test results of square specimens No.09, No.11, No.13 and No.15

3.3 Influence of cross-section slenderness

Fig. 8 and Fig. 9 show a comparison between circular and square CSFT of different cross-section slenderness subjected to monotonic and cyclic bending. All the four specimens were in-filled with rubberized concrete RuC15% and tested under simple bending. It could be concluded that, for the circular members, the specimens with both high and moderate cross-section slenderness exhibited similar ductility under monotonic and cyclic loading. The strength degradation under cyclic load was also similar for the two different cross-section slenderness, but it should be noted that specimen with higher cross-section slenderness developed low cycle fatigue earlier than the one with lower cross-section slenderness. For square CFST column under the cyclic load, little pinching effect was observed for the specimen with high cross-section slenderness and the development of strength degradation was not so pronounced in comparison to the specimen with higher cross-section slenderness. Thus, the cross-section slenderness of CFST members has a higher influence on the strength degradation of square columns than circular columns.

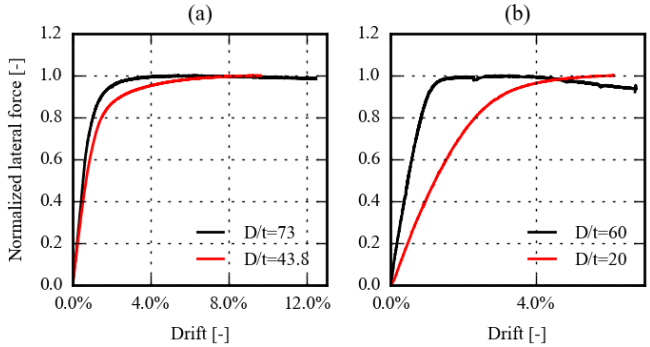

Fig. 8 – Comparison of circular (a) and square (b) CFST of different cross-section slenderness under monotonic bending

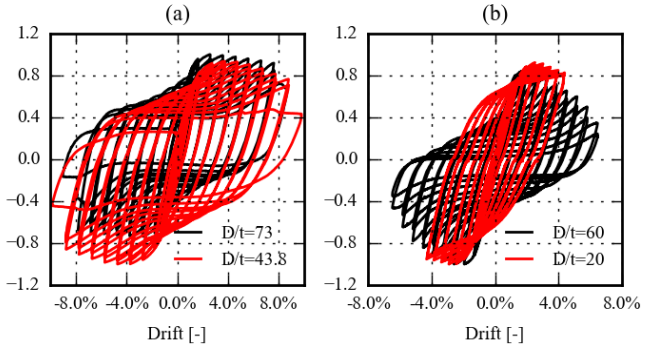

Fig. 9 – Comparison of circular (a) and square (b) CFST of different cross-section slenderness under cyclic bending

3.4 Influence of concrete type

Fig. 10 and Fig. 11 show a comparison between circular and square CFSTs with different in-filled concrete subjected to monotonic and cyclic bending. For all the specimens, the steel tube cross-section sizes are the same, namely C219×5 for circular CFSTs and S200×10 for square CFSTs. No axial load was applied to the specimens. It can be seen from the plots that, even though the standard concrete (StdC) has an uniaxial strength 150% higher than rubberized concrete (RuC15%), the increase of the member bending capacity is not that significant, as most of the resistance is developed by the steel tube composing the CFST section. It could be proved that the application of CFST combining low strength concrete and steel tube, as the infill of low strength concrete has limited influence on the member ductility.

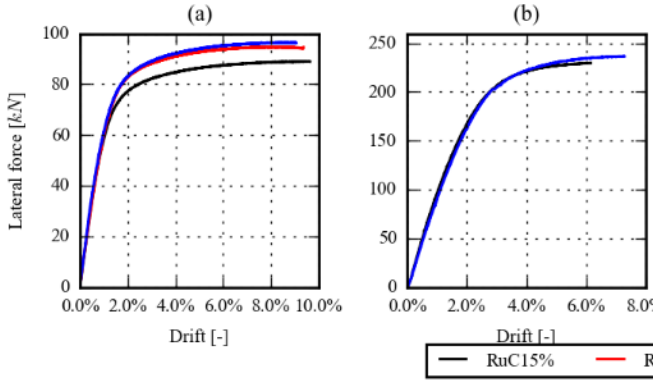

Fig. 10 – Comparison of circular (a) and square (b) CFST of different in-filled concrete under monotonic bending

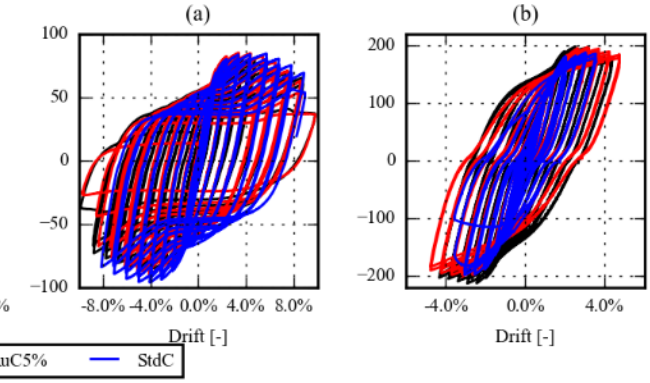

Fig. 11 – Comparison of circular (a) and square (b) CFST of different in-filled concrete under cyclic bending

4. Numerical modelling

The finite element software ABAQUS [3] was used to generate a 3D model. The model can not only consider the geometry nonlinearity, material nonlinearity during analysis, but also capture member behaviour, namely the local buckling of the steel tube wall, the bi-axial and tri-axial stress state of the materials, the contact behaviour between the steel tube and the concrete core. The experimental results are used to develop and calibrate the model. Parameters including finite element types, mesh size, geometry imperfection, material plasticity and instances interaction should be careful calibrated to make the model accurate and reliable. It is also important to consider the computational cost while pursuing the accuracy of the numerical results.

4.1 Finite element types, mesh and boundary conditions

Based on the CFST's composition, the CFST members were modelled with two different parts, namely the concrete core and the steel tube. Whilst the former is modelled with solid C3D8R finite element, the latter is modelled with shell S4R finite element, as shown in Fig. 12. According to the observations made during the experimental tests, the CFST members showed large values of section curvature and developed local buckling of steel tube at the plastic hinge zone. The remaining length of the specimens did not exhibit noticeable local deformations. In line with these observations, the members were modelled with a mixed mesh refinement, as shown in Fig. 12. For the bottom of the column, with a length of one external diameter of the CFST, d (or section height h for square and rectangular section), a more detailed mesh is used for both the steel and the concrete, with 20 finite element layers along the height. The remaining length of the column was meshed more sparsely, with 15 finite element layers. The cross-section mesh of the columns is shown in Fig. 13. A value of 20 was adopted for the equally spaced divisions along the perimeter of both the concrete core and steel tube cross-section, and 14 equally spaced divisions along the diameter of the concrete core cross-section.

Regarding the boundary conditions of the columns, the members were considered to be fully fixed at the bottom sections of both the concrete core and the steel tube. At the top, no boundary conditions were defined in ABAQUS in addition to an imposed lateral displacement and a constant vertical axial load. It is important to highlight, as already mentioned in Section 2 of this paper, that no $P-\Delta$ effects were generated during the experimental tests. Differently from the test, in ABAQUS, the axial load follows the movement of top cross-section while keeping the vertical direction, which will introduce additional moment to the base section. In order to fit accurately the tests' observation, this additional moment was converted to additional lateral force at the top when dealing with the numerical results.

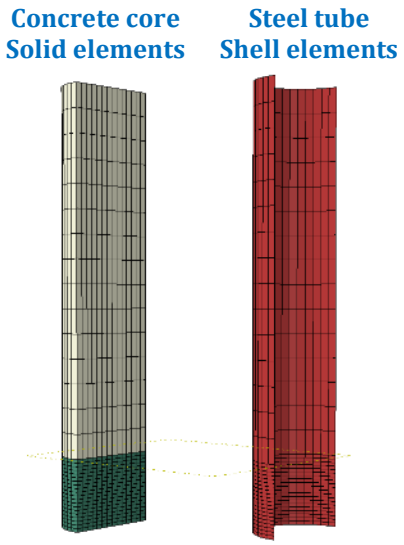

Fig. 12 – Geometry and mesh of the ABAQUS model

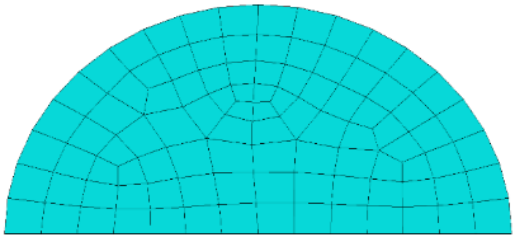

Fig. 13 – Section mesh discretization of the concrete instance

4.2 Surface contact interaction

Regarding the contact interaction between the concrete core and the steel tube, neither sliding nor separation between both surfaces was allowed to develop for the length of specimen above one CFST diameter, d (or section height h for square and rectangular section) based on observations made throughout the experimental tests. On the other hand, the bottom part of the specimens exhibited local buckling deformation of the steel tube. That could only could be possible if there is separation allowed between the surfaces. Thus, for the zone with a dense mesh, a "hard contact" behaviour was assigned to the normal direction of the surfaces, allowing for separation, but not penetration, between the two surfaces. For the tangential component, a Coulomb friction

model was adopted for the contact surface, in order to simulate the friction forces that develop when slippage occurs between the two surfaces. A value of 0.2 was adopted for the friction coefficient of the contact surface of the bottom length of the members.

4.3 Modelling of the steel material

For the elastic behaviour range of the steel tube material, a Young modulus, E_s, of 200GPa (Han *et al* [6]) and a Poisson ratio, ν, equal to 0.3 (Elloboday *et al* [7]) were adopted. As for the material inelasticity, a nonlinear isotropic/kinematic model was adopted, dependent on the yield stress, f_y, a set of kinematic hardening factor, C_i, and the isotropic factor, γ_i. The values of f_y, obtained from tensile coupon testing of steel tube samples, for each test member, are shown in Table 3. The number of sets C_i and γ_i was fixed to 1 and the corresponding values of each steel tube are shown in Table 5.

Table 5 – Values of C and γ of each steel tube

Steel tube section	**C219×3**	**C219×5**	**S180×3**	**S200×10**	**R250×150×12**
C [MPa]	1700	3700	2500	1500	1500
γ	10	20	15	12	20

4.4 Modelling of the concrete material

To what concerns the material modelling of the concrete core of the CFST members, a Poisson ratio, ν, equal to 0.2 and a Young modulus, E_c, given by Eq. (1) were adopted (ACI 318-11 [8]).

$$E_c = 4700\sqrt{f_c} \tag{1}$$

For the concrete plasticity, the concrete damaged plasticity model available in ABAQUS is adopted, as it is generally capable of modelling the inelastic behaviour of concrete and other quasi-brittle materials for various structural members. It is important to note that the parameters of the concrete damaged plasticity model could not be obtained directly from testing of concrete cube samples. As such, the values available either from previous research or adopted during the model calibration were used in the present research.

Concerning the flow potential eccentricity (ϵ), and the viscosity parameter (μ), the default values recommended by ABAQUS were used in the concrete damage plasticity model, namely $\epsilon = 0.1$ and $\mu = 0$. Additionally, for the dilation angle (ψ), a value of 30º was adopted as it fits well with the test data. Concerning the ratio f_{b0}/f_{c0}, the formulation adopted by Papanikolaou and Kappos [9]was followed for the current concrete material model, as shown by Eq. (2).

$$f_{b0}/f_{c0} = 1.5 f_c^{\,-0.075} \tag{2}$$

Finally, the computation of K_c is accomplished with the proposal made by Yu *et al* [10], expressed as Eq. (3).

$$K_c = \frac{5.5 f_{b0}}{3f_{c0} + 5f_{b0}} = \frac{5.5}{5 + 2f_c^{0.075}} \tag{3}$$

It should be noted that, in Eq. (1), Eq. (2) and Eq. (3), the f_c should be in MPa units.

In addition to the aforementioned material modelling parameters, the concrete's uniaxial post-yield stress-strain constitutive law, both in compression and tension were adopted, as shown in Fig. 14 and Fig. 15.

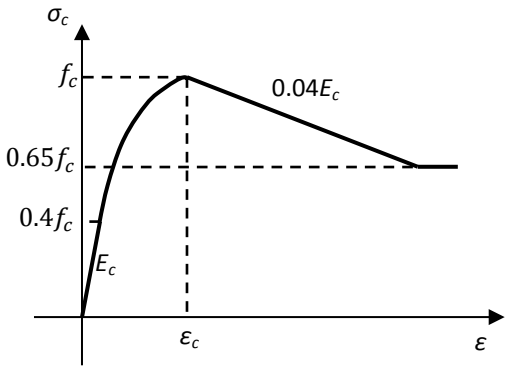

Fig. 14 – Constitutive law proposed for concrete in compression

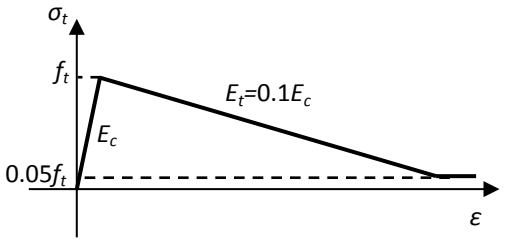

Fig. 15 – Constitutive law proposed for concrete in tension

Based on the proposal of Eurocode 2 [11] for concrete under compression, the material uniaxial behaviour used in this research may be divided into four stages. Firstly, an elastic range in which the stress, σ_c, increases linearly with the strain, ε, according to the Young modulus, E_c, up to 40% of the yield compressive strength, f_c. In the second stage, σ_c increases nonlinearly with ε until the peak stress is reached, namely for $\sigma_c = f_c$ and $\varepsilon = \varepsilon_c$, and is given by Equation (4). For obvious reasons, the softening behaviour defined in the code will not be directly applicable to CFST members, as the encasing steel tube delays the cracking development and hence the failure of the material. Thus, differently from Eurocode 2 [11], the third stage of Fig. 14 was defined with a linear decrease of σ_c, with a gradient of $-0.04E_c$, until 65% of the compressive strength of the concrete is reached. Finally, for higher levels of strain, the concrete was considered to have a constant residual strength of $0.65f_c$.

$$\frac{\sigma_c}{f_c} = \frac{k\eta - \eta^2}{1 + (k-2)\eta} \tag{4}$$

Where: $= \varepsilon/\varepsilon_c$, $\varepsilon_c = 2\, f_c/E_c$, $k = 1.05\, E_c\varepsilon_c/f_c$

Regarding the uniaxial tensile behaviour of the concrete, the maximum stress value in tension, f_t, was considered as 10% of the compressive strength ($0.1f_c$). Up to this point, the stress-strain curve increases linearly with the same gradient as the first stage of Fig. 15, i.e. E_c. For higher strain levels, softening starts to develop in the material with a tangent slope of $E_t = -0.1E_c$, until reaching 5% of f_t. A residual tensile strength of $\sigma_t = 0.05f_t$ was adopted in the numerical model.

4.5 Cracking configuration for a member subjected to cyclic bending

Under bending, the concrete core will develop cracking and gaps will open. During cyclic loading, the gap will open on the tension side and close on the compression side, which will introduce pinching effects. However, with the solid element in ABAQUS, it is not possible to develop the cracking as the mesh is fully continuous. Thus, in order to capture the pinching effect, cracking is pre-defined in the plastic zone of CFST members with a uniform distribution of 2cm spacing. The ultimate cracking width and the tension stress is defined as 0.1mm and $0.1f_c$, which means the cracking will develop when stress is over $0.1f_c$ and loss contact when cracking width is larger than 0.1mm.

5. Validation of the numerical model and Eurocode 4

In order to validate the 3D element model, the experimental tests described in Section 2 of this paper were numerically simulated.

Fig. 16 shows a comparison of the local buckling mechanisms developed both in experimental test and in numerical simulation, for circular CFST No. 4 and square CFST No. 9. The 3D element model was able to accurately capture the local buckling deformation at the member's fixed base level, both in terms of amplitude, shape and location along the specimen height.

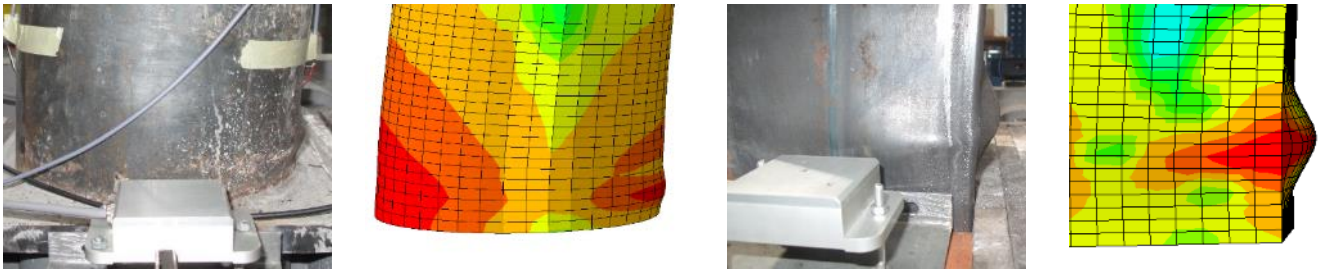

Fig. 16 – Local buckling mechanisms of the experimental test and the 3D element model

Concerning the global behaviour of the members, Fig. 17 and Fig. 18 show a comparison of the lateral force-deformation curves obtained for the test specimens with those provided by the numerical model. It can be concluded that, overall, the numerical model can capture both the elastic and post-yield behaviour, namely the ultimate lateral force and the member bending ductility. For the specimen under cyclic test, the pinching effect and the strength degradation could also be reproduced by the numerical model.

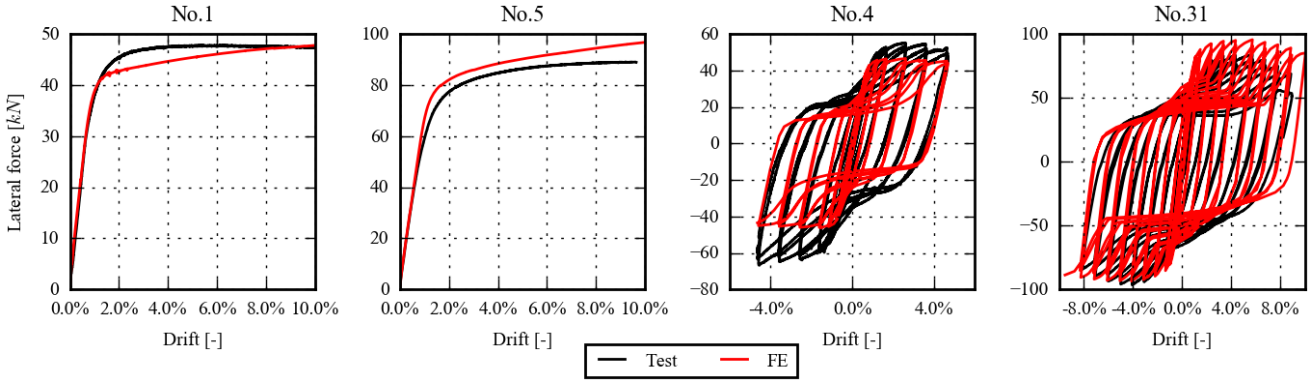

Fig. 17 – Comparison between numerical model and test results of circular specimens No.01, No.05, No.04, No.31

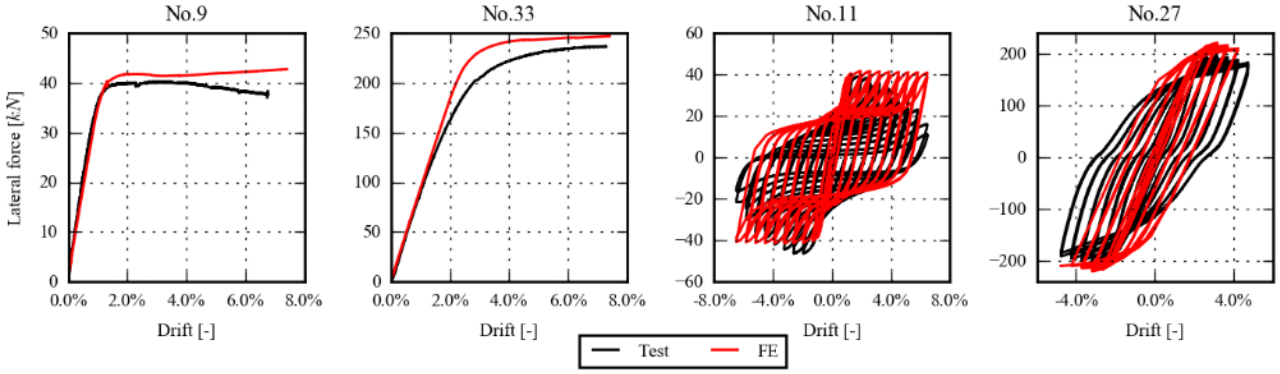

Fig. 18 – Comparison between numerical model and test results of square specimens No.09, No.33, No.11, No.27

The ultimate base moment observed from the test results (M_{test}), analytical results (M_{FE}) under monotonic load and their corresponding design capacity based on Eurocode 4 [2] (M_{EC4}) are listed in Table 6. The table allows concluding that the numerical model provides an accurate prediction of the CFST flexural behaviour with a mean difference of 1% for circular section and 8% for square and rectangular section. Regarding Eurocode 4, the design capacities are always conservative in comparison to the experimental results, with a mean difference of 24% for the circular members and 13% for square and rectangular members. The mean difference of bending capacities illustrates that, the circular CFST is associated with the development of an overstrength effect, which results in a more conservative prediction by Eurocode 4 in comparison to the square/rectangular CFST members. The possible reason for the overstrength may be the concrete confinement

effect, as the circular steel tube provides more confinement to the concrete core, thus enhancing the compressive strength of the material, in comparison to the square/rectangular steel tubes. However, as mentioned in Section 3, the concrete has a lower contribution to the bending resistance in comparison to the steel tube, which indicates that the overstrength phenomenon is also associated to the behaviour of the steel tube. Ongoing research is focusing on the study of the possible factors responsible for the overstrength observed on the circular CFSTs.

Table 6 – Ultimate capacity comparison between Eurocode 4 [2], numerical model and test results

Circular CFST						Square and rectangular CFST					
Specimen #	M_{test} [kNm]	M_{EC4} [kNm]	M_{FE} [kNm]	$\frac{M_{EC4}}{M_{test}}$	$\frac{M_{FE}}{M_{test}}$	Specimen #	M_{test} [kNm]	M_{EC4} [kNm]	M_{FE} [kNm]	$\frac{M_{EC4}}{M_{test}}$	$\frac{M_{FE}}{M_{test}}$
1	64.5	48.7	64.8	0.75	1.00	9	54.4	51.6	57.7	0.95	1.06
2	74	53.8	67.5	0.73	0.91	10	41.9	54.5	60.3	1.3	1.44
5	120.2	93.9	131.0	0.78	1.09	13	310.2	237.2	315.8	0.76	1.02
6	134.6	98.3	125.6	0.73	0.93	14	283.5	239.4	314.1	0.84	1.11
21	127.9	99	137.7	0.77	1.08	25	361.9	245.3	325.7	0.68	0.90
22	139.1	106.9	136.4	0.77	0.98	26	312.9	250.6	329.0	0.8	1.05
29	130.3	101.6	141.8	0.78	1.09	33	319.8	249.9	333.5	0.78	1.04
30	142.2	111.4	144.5	0.78	1.02	34	305.2	256.3	341.2	0.84	1.12
						17	351.7	286.4	338.9	0.81	0.96
						18	311.9	287.2	334.5	0.92	1.07
			μ	0.76	1.01				μ	0.87	1.08
			σ	0.02	0.06				σ	0.17	0.14

6. Conclusions

In total, 36 CFST specimen with different parameters, namely section shape, section size, steel properties, concrete properties and load condition had been selected and tested under monotonic/cyclic bending. A numerical model of the specimens was developed and calibrated. Validation of the numerical model and Eurocode 4 design provisions was also presented in this paper. The main conclusions of the research are:

- The experimental tests demonstrated the high ductility of CFST members, even for D/t ratios higher than the current limit prescribed in Eurocode 8;
- The concrete type (StdC vs RuC) has little influence on the local buckling and member ductility of CFST columns' flexural, which indicates the feasibility of using rubberized concrete in CFST;
- Larger section slenderness reduces post-yield hardening behaviour for rectangular and square members but has little influence on circular members;
- The numerical model developed in ABAQUS was able to reproduce with high accuracy the test results;
- Eurocode 4 provides conservative estimates of the bending capacity of CFST members in comparison to the test results;
- An important overstrength was observed for circular CFSTs under monotonic bending which can be partially justified by concrete confinement effects.

7. Acknowledgments

The authors would like to acknowledge the Portuguese Foundation for Science and Technology (FCT) for the financial support through the research project "Recycling & Seismic Protection: Sustainable High-Performance CFST Columns for Seismic Areas" (PTDC/ECM/117774/2010). Also acknowledged is the support of FERPINTA, by providing all the steel tubes for the experimental campaign, and PRESDOURO, for providing the resources for the casting of the concrete of the specimens. This work was also supported by FCT, through IDMEC, under LAETA, project UID/EMS/50022/2013

8. References

[1] Silva A, Jiang Y, Castro J.M, Silvestre N, Monteiro R (2016): Experimental assessment of the flexural behaviour of circular rubberized concrete-filled steel tubes. *Journal of Constructional Steel Research*, **122**, 557-570.

[2] CEN, EN 1994-1-1 Eurocode 4 (2004): Design of composite steel and concrete structures. Part 1-1, General rules and rules for buildings. *European Commitee for Standardization, Brussels, Belgium, 2004a.*

[3] ABAQUS (2011): ABAQUS Documentation. *Dassault Systèmes Simulia Corp*., Providence, RI, USA.

[4] CEN, EN 1998-1 Eurocode 8 (2004): Design of structures for earthquake resistance. Part 1, General rules, seismic actions and rules for buildings. *European Commitee for Standardization, Brussels, Belgium, 2004b.*

[5] SAC (1997): Protocol for fabrication, inspection, testing, and documentation of beam-column connection tests and other experimental specimens, *Rep. No. SAC/BD-97, 1997, 2.*

[6] Hu H.T, ASCE M., Huang C.S, Wu M.H, Wu Y.M, (2003): Nonlinear Analysis of Axially Loaded Concrete-Filled Tube Columns with Confinement Effect. *Journal of Structural Engineering*, **129** (10), 1322-1329.

[7] Ellobody E, Young B, Lam D (2006): Behaviour of normal and high strength concrete-filled compact steel tube circular stub columns. *Journal of Constructional Steel Research*, **62**, 706–715.

[8] American Concrete Institute (2011): Building Code Requirements for Structural Concrete (ACI 318-11) and Commentary. *MI, USA: Farmington Hills*

[9] Papanikolaou V.K, Kappos A.J (2007): Confinement-sensitive plasticity constitutive model for concrete in triaxial compression. *International Journal of Solids and Structures*, **44**, 7021-7048

[10] Yu T, Teng J.G, Wong, Y.L, Dong, S.L (2010): Finite element modeling of confined concrete-I: Drucker–Prager type plasticity model. *Engineering Structures*, **32**, 665-679

[11] CEN, EN 1992-1-1 Eurocode 2 (2004): Design of concrete structures. Part 1-1: General rules and rules for buildings, *European Commitee for Standardization, Brussels, Belgium, 2004b.*